Supplementary Information

High-performance magnetic metal microrobot prepared by two-photon polymerization and sintering method†

Rui Li,‡[a] Modong Jiang,‡[a] Bingrui Liu,[a] Shaojun Jiang,[a] Chao Chen,[b] Mengxue Liang,[c] Lijie Qu,[a] Chaowei Wang,[a] Gang Zhao,[a] Yanlei Hu,[a] Dong Wu,[a] Jiaru Chu,[a] Jiawen Li*[a]

[a] CAS Key Laboratory of Mechanical Behavior and Design of Materials, Key Laboratory of Precision Scientific Instrumentation of Anhui Higher Education Institutes, Department of Precision Machinery and Precision Instrumentation, University of Science and Technology of China, Hefei 230027, China.

[b] Department of Materials Physics and New Energy Device, School of Materials Science and Engineering, Hefei University of Technology, Hefei 230009, China

[c] CAS Key Laboratory of Urban Pollutant Conversion, Department of Environmental Science and Engineering, University of Science and Technology of China, Hefei 230026, China

E-mail: (jwl@ustc.edu.cn)

‡These authors contributed equally to this paper.

This PDF file include:

Move S1 to S5
Note S1 to S4
Figure S1 to S12

Note S1. The shape parameter (SP) of microhelix

The shape parameters of polymer-based microhelixes before sintering (mainly including the radius R and pitch P) have a significant impact on the Ni-MAR after sintering. Here we define a shape parameter (SP) to divide these microhelixes with different radiuses and pitches into three types:

$$\mathrm{SP} = \sqrt{(\frac{R}{P})^2 + (\frac{P}{R})^2}$$

As is shown in Fig S7, when the SP is bigger than 7, the Ni-MAR is slim. When the SP is bigger than 3 and less than 7, the Ni-MAR is moderate. When the SP is less than 3, the Ni-MAR is dumpy.

Note S2. Preparation of solution with different viscosity

Glycerol and DI water are mixed together in different proportions according to the viscosity data for aqueous glycerol solutions. The operating temperature is 30 ℃. Therefore, the viscosity of DI water without glycerol is 0.8 CP. The 4 CP solution is obtained by adding 50 wt% glycerol into the DI water and the 118 CP solution is acquired by adding 90 wt% glycerol into the DI water.

Note S3. Calculation of the mass of Ni-MAR and microcube

After experimentally measurement, the organic-inorganic Ni-based photoresin and SZ2080 have approximately equal density. Here we define their density as ρ in the following calculation. According to the material component, the mass fraction of nickel element in the organic-inorganic Ni-based photoresins can be calculated as

$$Ni\ wt\% = \frac{mass\ of\ nickel}{total\ mass} = \frac{1290 * 5\% * \frac{58.69}{208.86}}{100 + 1290 * 95\% * 40\% + 300 + 12} \approx 2\ wt\%$$

The mass of Ni-MAR after sintering and reduction, is approximately equal to the mass of nickel element in the polymer-based microhelix (wire radius in 2.5 μm, spiral radius in 7 μm, spiral pitch in 30 μm, and spiral number in 2). Therefore, the mass of Ni-MAR is

$$Ni - MAR = m * Ni\ wt\% = V\rho * Ni\ wt\% = \pi r^2 l\rho * Ni\ wt\%$$

$$= 3.14 * 2.5^2 * \sqrt{(3.14 * 7 * 2)^2 + 30^2} * 2 * \rho * 2\% = 41.7\rho$$

In the meanwhile, the mass of microtube can be figured out as

$$microcube = V\rho = 20^3\rho = 8000\rho$$

Hence, a microcube is about 200 times heavier than the Ni-MAR.

Note S4. Theoretical model to explain the massive cargo carrying of Ni-MAR

The forces on the microcube are comprised of two types: propulsion force (F_P) and drags force (F_D).

$$F_P = F_D$$

1.1 Drag force (F_D)

A moving microcube in a viscous solution will be dragged by the friction force (F_f, between the microcube and substrate) and the drag force (F_d, between the microcube and the solution).

$$F_D = F_f + F_d$$

The friction force can be calculated by

$$F_f = \mu mg$$

Where the μ is the friction coefficient. Our microcube is immersed in liquid and moves on the surface of substrate. For polymer moving on a substrate, the μ is generally between 0.01 and 0.1.[1] Here, the μ is set as 0.05. Besides, the m is the mass of microcube.

$$m = v\rho$$

Where the v is the volume of microcube, which can be calculated as $v = (20 * 10^{-6})^3 = 8 * 10^{-15}\ m^3$. The ρ is the density of microcube, which is measured to be $1.2 * 10^3\ kg/m^3$.

Therefore, the friction force is

$$F_f = 0.05v\rho g = 4.8 * 10^{-12}\ N$$

The drag force can be calculated by

$$F_d = \frac{1}{2} C_d A \rho V^2$$

Where A is the area of the moving microcube facing the liquid, which can be calculated as $A = (20 * 10^{-6})^2 = 4 * 10^{-10}\ m^3$. The V is the velocity of microcube ($V = 4.8 * 10^{-7}\ m/s$ in Fig. 5e). The C_d is the drag coefficient. For a polymer cube in water, the C_d is around 1.05. [2]

Therefore, the drag force is

$$F_d = \frac{1}{2} * 1.05 * 4 * 10^{-10} * 1.2 * 10^3 * (4.8 * 10^{-7})^2 \approx 5.8 * 10^{-20}\ N$$

Obviously, the $F_d \ll F_f$. Therefore,

$$F_D \approx F_f = 4.8 * 10^{-12}\ N$$

1.2 Propulsion force (F_P)

For our helical Ni-MAR in a rotating magnetic field, the produced propulsion force

in the long axis can be calculated as[3]

$$F_P = \int_0^{n\lambda} dF_p = n\lambda w\sigma sin\theta(\zeta_\perp - \zeta_\parallel)$$

Where the n is the number of helical turns. Here, the n is 2 for our Ni-MAR. The λ is the pitch, which is 10 μm. The w is the angular velocity of the Ni-MAR. In Fig 5, the Ni-MAR pushes the microcube with a frequency of 25 HZ. Hence, the w equals 50π rad/s. The σ is the radius of Ni-MAR, which is 2 μm. The θ is the helix angle. The $tan\theta = 2\pi\sigma/\lambda = 0.3\pi$. Hence, the $sin\theta$=$(tan^2\theta/(tan^2\theta + 1))^{1/2}$=0.69. The $\zeta_\perp$ and $\zeta_\parallel$ are the drag coefficients, which are given by[4]

$$\xi_\perp = \frac{4\pi\eta}{\ln\left(\frac{0.36\pi\sigma}{rsin\theta}\right) + 0.5}$$

$$\xi_\parallel = \frac{2\pi\eta}{\ln\left(\frac{0.36\pi\sigma}{rsin\theta}\right)}$$

Where the r is the diameter of helical filament. The η is the dynamic viscosity. For our Ni-MAR swimming in the liquid, the η equals about $1.01 * 10^{-3}\ Pa \cdot s$. Hence, we can get the values of $\zeta_\perp$ and $\zeta_\parallel$.

$$\xi_\perp = \frac{4\pi * 1.01 * 10^{-3}}{\ln\left(\frac{0.36\pi * 1}{0.5 * 0.69}\right) + 0.5} \approx 7.5 * 10^{-3}$$

$$\xi_\parallel = \frac{2\pi * 1.01 * 10^{-3}}{\ln\left(\frac{0.36\pi * 1}{0.5 * 0.69}\right)} \approx 5.3 * 10^{-3}$$

Finally, the propulsion force can be calculated as

$$F_P = 2 * 10 * 10^{-6} * 50\pi * 1 * 10^{-6} * 0.69 * (7.5 - 5.3) * 10^{-3} \approx 4.76 * 10^{-12}\ N$$

1.3 Drag force (F_D) and propulsion force (F_P)

The propulsion force F_P is almost equal to the drag force F_D, which means the

Ni-MAR can push a microcube with the maximum weight of 200 times the microrobot. If the microcube is heavier, for example 300 times the microrobot, the propulsion force of the Ni-MAR is less than the drag force of microcube, thus cannot push the microcube.

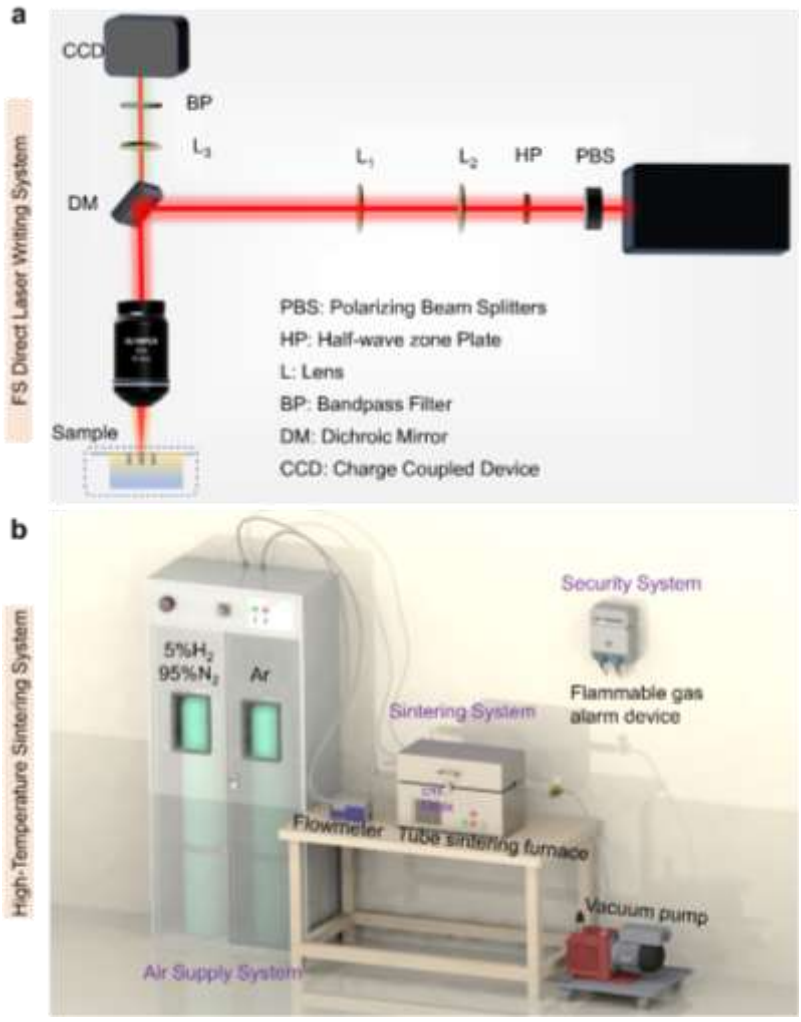

Fig. S1 Schematic diagram of femtosecond direct laser writing system (a) and high-temperature sintering/reduction system (b).

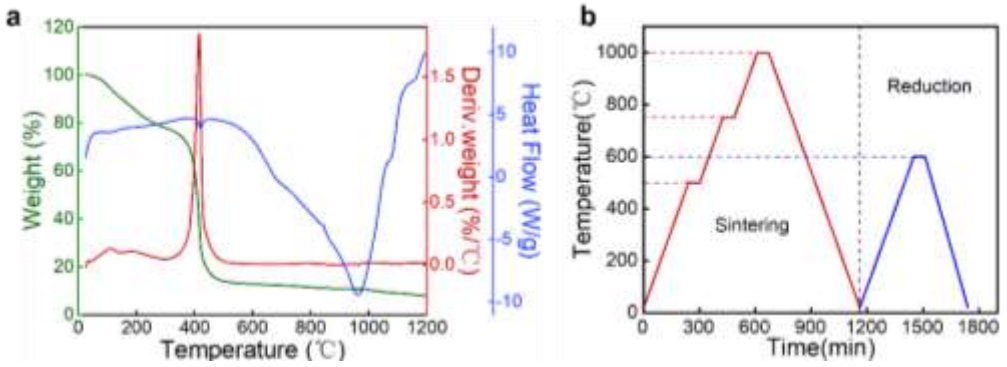

Fig. S2 (a) Thermo gravimetric analysis (TGA) and differential scanning calorimetry (DSC) profiles for heating of polymerized Ni-containing photoresist. (b) The heating profile.

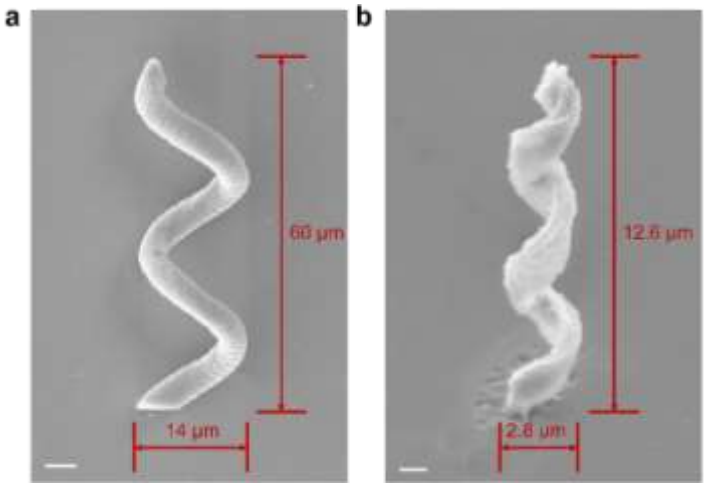

Fig. S3 SEM images of polymer-based microhelix (a) and pyrolyzed helical microrobot (b). Scale bars are 5 μm in (a) and 1 μm in (b). The dimensional shrinkage during the sintering process is about 80%.

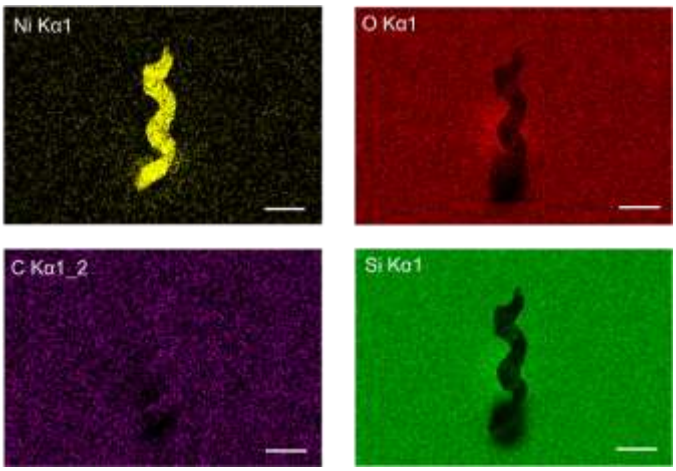

Fig. S4 Energy dispersive spectroscopy (EDS) mapping of fabricated Ni-MAR on a quartz glass substrate. Scale bar: 5 μm.

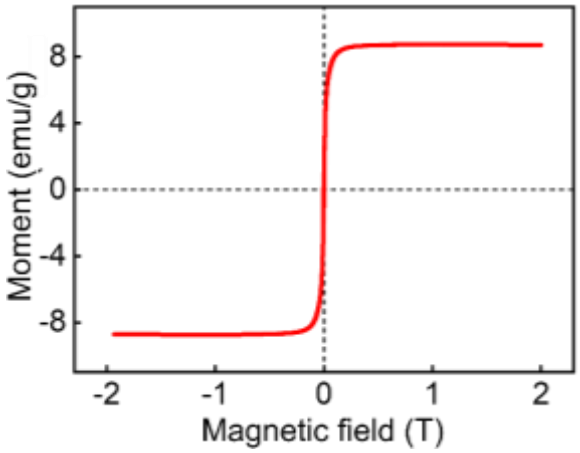

Fig. S5 The magnetic hysteresis loop of Ni-MAR.

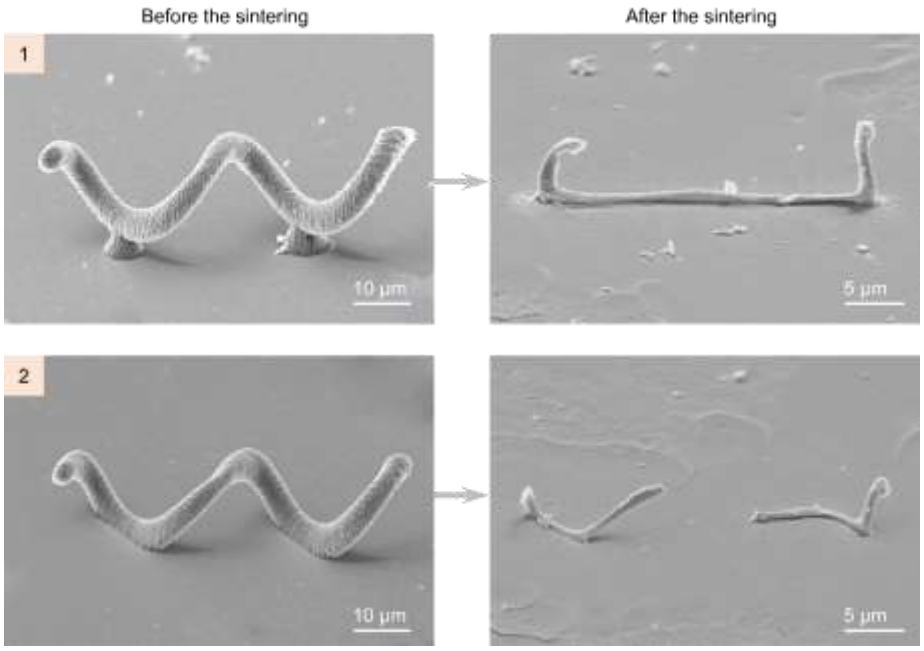

Fig. S6 SEM images of microhelixes with different contact forms before and after the sintering. These pyrolytic Ni-MARs cannot keep their initial shapes due to dramatic shrinking and structural distortions.

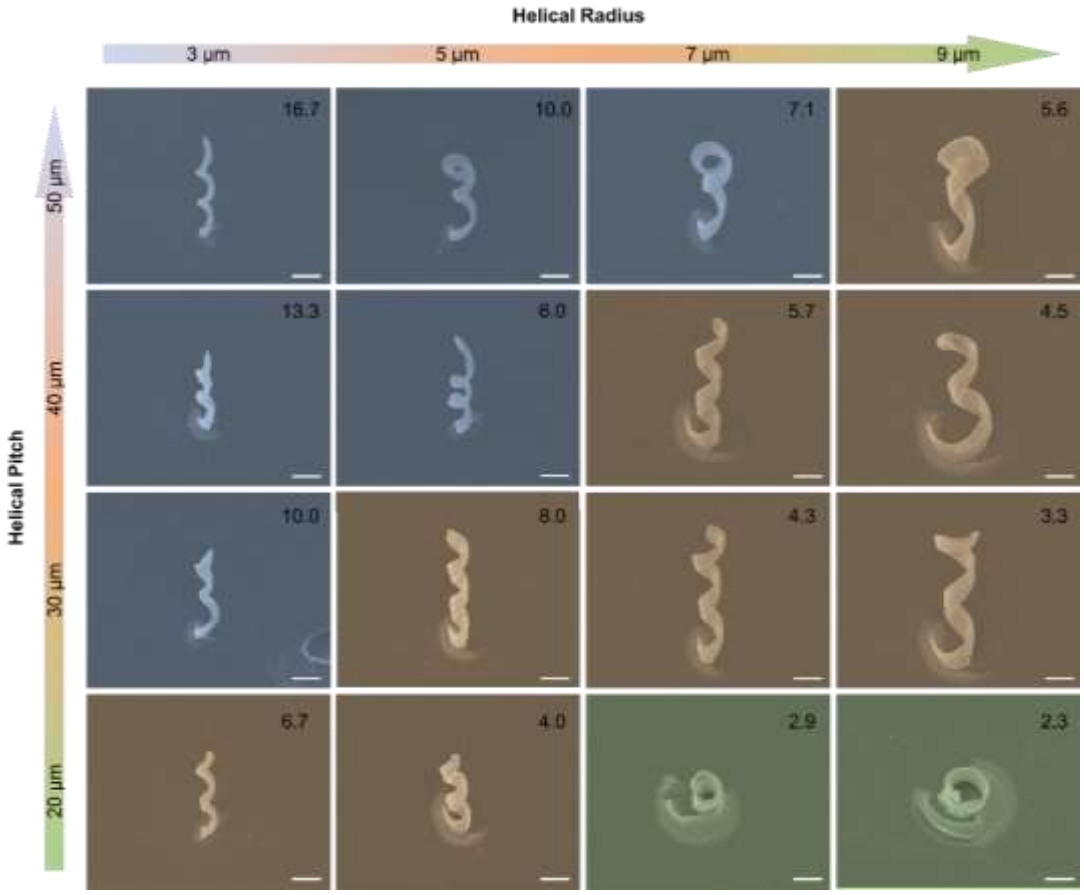

Fig. S7 SEM images of pyrolyzed helical Ni-MAR under different shape parameters. The helical radius of polymer-based microhelix increases from 3 μm to 9 μm, and the helical pitch of polymer-based microhelix increases from 20 μm to 50 μm. Scale bar: 5 μm.

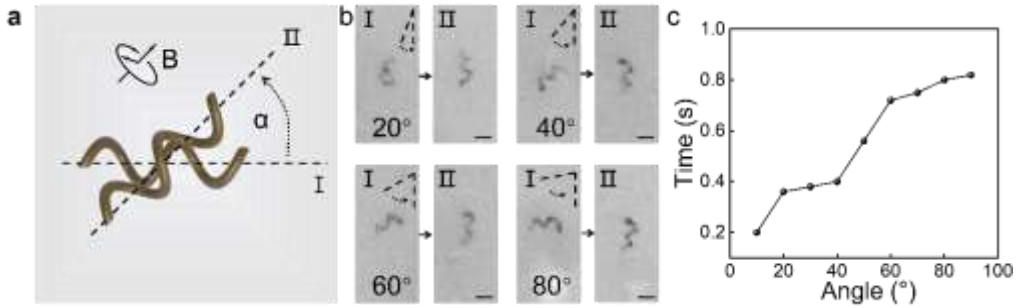

Fig. S8 The controllability of Ni-MAR with different step response. (a) The angle between the initial direction of Ni-MAR (I) and the direction of magnetic field (II). The rotating time of Ni-MAR from direction (I) to direction (II) is chosen to evaluate the controllability of Ni-MAR. The shorter the rotating time, the more controllable of the Ni-MAR. (b) The Ni-MAR aligning well with the external magnetic field with increased angle from 20° to 80°. Scale bar: 10 μm. (c) Rotating time with the angle changing from 10° to 90°, which are all less than 1s.

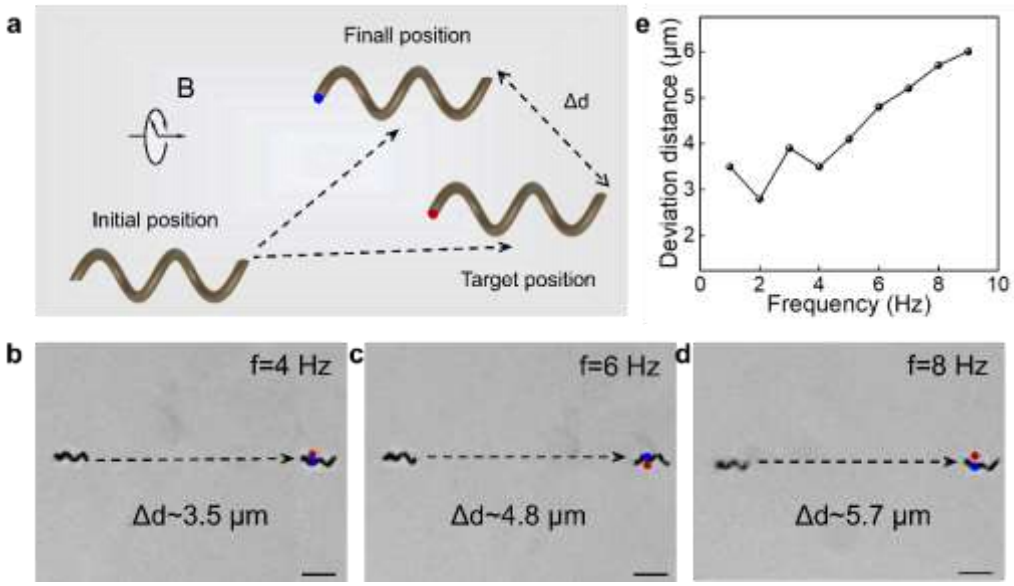

Fig. S9 The controllability of Ni-MAR under different frequencies of magnetic field. (a) The deviation distance (Δd) between the final position and target position of Ni-MAR, which shows the positioning accuracy of our microrobot. The blue dot and red dot denote the final position and target position of the Ni-MAR, respectively. (b-d) The swimming trajectory of Ni-MAR under different frequencies (f=4, 6, 8 Hz). The distance of initial position and the target position is set to be 150 μm. Scale bar: 20 μm. (e) The deviation distance of Ni-MAR under different frequencies of magnetic field. All the deviation distances are less than 6 μm. The Ni-MARs swim in a viscous solution (118 CP).

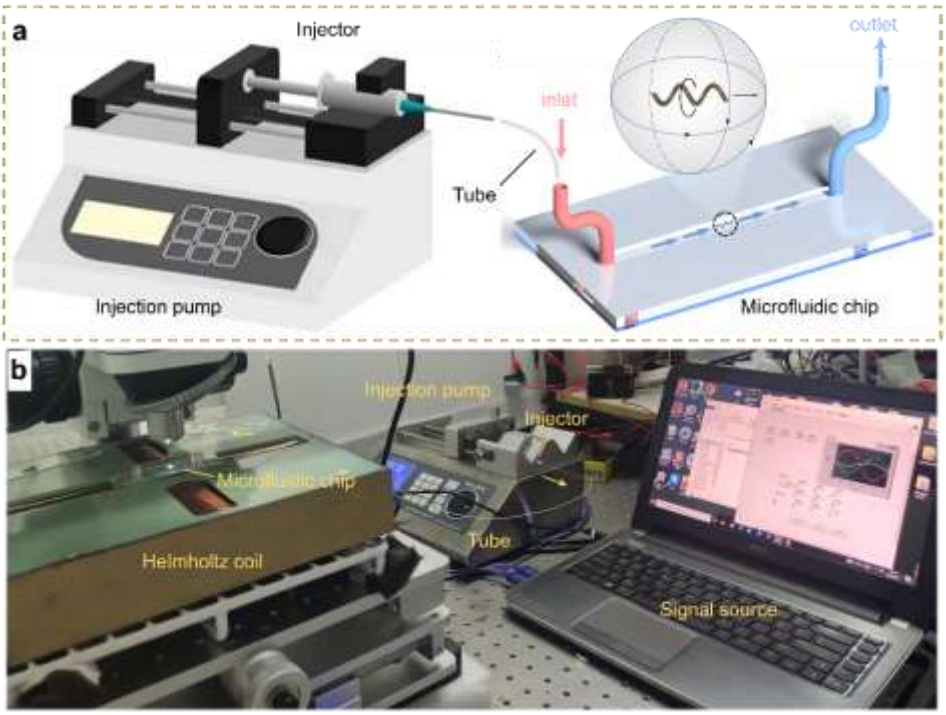

Fig. S10 The microfluidic system and magnetic actuation system. (a) Schematic diagram of the setup to perform the swimming test of Ni-MAR in a microfluidic channel. (b) The real picture of setup, composed of a magnetic actuation system and a microfluidic system. The microfluidic system consists of a microfluidic chip, an injector and an injection pump. The magnetic actuation system is mainly comprised of a signal source, a Helmholtz coil.

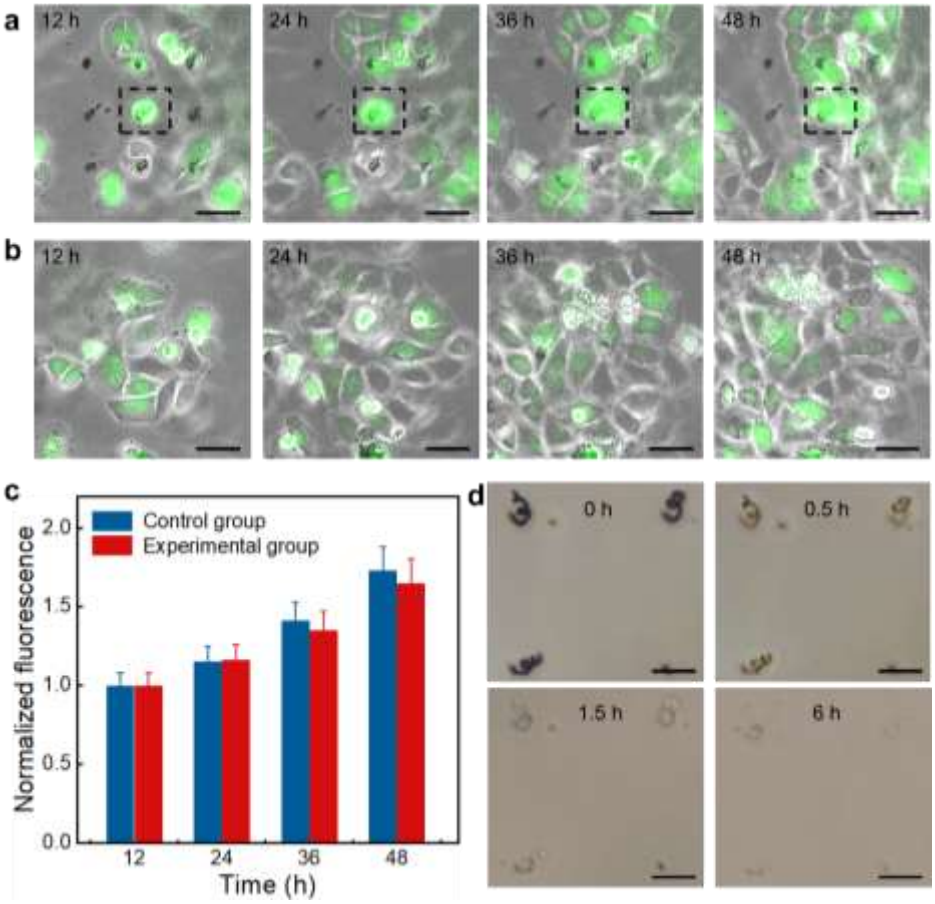

Fig. S11 The viability test by culturing cells with Ni-MAR array. (a) Snapshots of the viability of HeLa cells cultured with Ni-MAR array in experimental group. (b) Snapshots of the viability of HeLa cells cultured without Ni-MAR array in control group. (c) Quantitative statistics of normalized fluorescent area during cell culturing in experimental group and control group. (d) The degradation process of Ni-MAR in simulated gastric fluid. Scale bars are 20 μm.

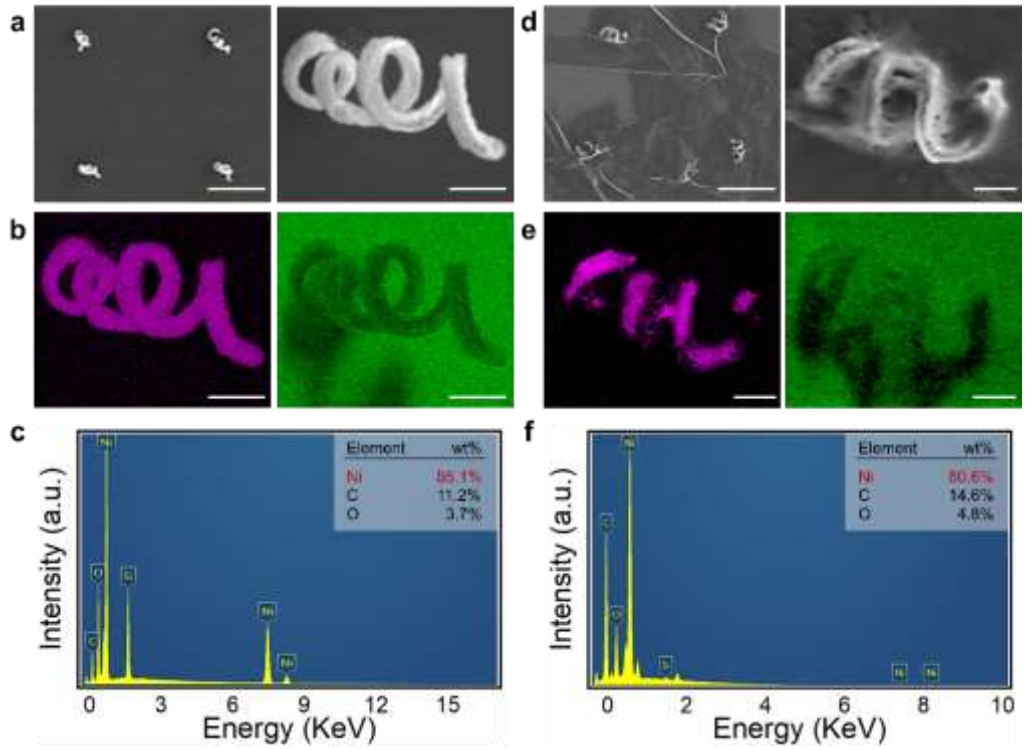

Fig. S12 The 3D morphology and elements content of Ni-MAR before and after the cell culturing. The SEM images (a) and EDS mappings (b) of Ni-MAR before the cell culturing. (c) The elements content of Ni-MAR before the cell culturing. The SEM images (d) and EDS mappings (e) of Ni-MAR after the cell culturing. (f) The elements content of Ni-MAR after the cell culturing. Scale bars are 25 μm in Ni-MAR array and 2.5 μm in single Ni-MAR.

Supplementary movies:

Movie S1. High-speed swimming of Ni-MAR.

Movie S2. The controllability of the Ni-MAR.

Movie S3. The controllable locomotion of Ni-MAR in flowing fluid inside a microfluidic chip.

Movie S4. A massive microcube pushed by a swimming Ni-MAR.

Movie S5. Ni-MAR pushing cells.

Reference:

1. Bartenev, G. M.; Lavrent′ev, V. V. a. c., *Friction and wear of polymers*. Elsevier: 1981; Vol. 6.
2. Çengel, Y. A.; Turner, R. H.; Cimbala, J. M.; Kanoglu, M., *Fundamentals of thermal-fluid sciences*. McGraw-Hill New York: 2001; Vol. 703.
3. Wang, L.; Xu, H.; Zhai, W.; Huang, B.; Rong, W., Design and characterization of magnetically actuated helical swimmers at submillimeter-scale. *Journal of Bionic Engineering* **2017,** *14* (1), 26-33.
4. Lighthill, J., Flagellar hydrodynamics. *SIAM review* **1976,** *18* (2), 161-230.